

Minerva Access is the Institutional Repository of The University of Melbourne

Author/s:

Wan, S;Kelly, PM;Mahon, E;Stöckmann, H;Rudd, PM;Caruso, F;Dawson, KA;Yan, Y;Monopoli, MP

Title:

The "sweet" Side of the protein corona: Effects of glycosylation on nanoparticle-cell interactions

Date:

2015-02-24

Citation:

Wan, S., Kelly, P. M., Mahon, E., Stöckmann, H., Rudd, P. M., Caruso, F., Dawson, K. A., Yan, Y. & Monopoli, M. P. (2015). The "sweet" Side of the protein corona: Effects of glycosylation on nanoparticle-cell interactions. *ACS Nano*, 9 (2), pp.2157-2166. <https://doi.org/10.1021/nn506060q>.

Persistent Link:

<https://hdl.handle.net/11343/90867>

The “Sweet” Side of the Protein Corona: Effects of Glycosylation on Nanoparticle-Cell Interactions

Sha Wan,[‡] Philip M. Kelly,[‡] Eugene Mahon,[‡] Henning Stöckmann,[†] Frank Caruso,[#] Kenneth A. Dawson,[‡] Yan Yan,^{#,} and Marco P. Monopoli^{‡,*}*

[‡]Centre for BioNano Interactions, School of Chemistry and Chemical Biology, University College Dublin, Dublin 4, Ireland, [†]NIBRT, GlycoScience Group, NIBRT-The National Institute for Bioprocessing Research and Training, Fosters Avenue, Mount Merrion, Blackrock, Co. Dublin, Ireland, and [#]ARC Centre of Excellence in Convergent Bio-Nano Science and Technology, and the Department of Chemical and Biomolecular Engineering, The University of Melbourne, Parkville, Victoria 3010, Australia.

*AUTHOR EMAIL ADDRESS: marco.monopoli@cbni.ucd.ie, yanyan@unimelb.edu.au

KEYWORDS: nanoparticle, glycosylation, protein corona, macrophage, adhesion, internalization

1
2
3 ABSTRACT
4
5

6 The significance of a protein corona on nanoparticles in modulating particle properties and their
7 biological interactions has been widely acknowledged. The protein corona is derived from
8 proteins in biological fluids, many of which are glycosylated. To date, the glycans on the
9 proteins have been largely overlooked in studies of nanoparticle-cell interactions. In this study,
10 we demonstrate that glycosylation of the protein corona plays an important role in maintaining
11 the colloidal stability of nanoparticles and influences nanoparticle-cell interactions. The removal
12 of glycans from the protein corona enhances cell membrane adhesion and cell uptake of
13 nanoparticles in comparison with the fully glycosylated form, resulting in the generation of a
14 pro-inflammatory milieu by macrophages. This study highlights that the post-translational
15 modification of proteins can significantly impact nanoparticle-cell interactions by modulating the
16 protein corona properties.
17
18
19
20
21
22
23
24
25
26
27
28
29
30
31
32
33
34
35
36
37
38
39
40
41
42
43
44
45
46
47
48
49
50
51
52
53
54
55
56
57
58
59
60

1
2
3 Advances in engineering functional structures at the nanoscale have led to the generation of a
4 wide range of nanoparticles, including silica (SiO₂) nanoparticles, gold nanoparticles, and
5 polymeric nanoparticles.¹ With their dimension in the size ranging from 1 – 100 nm, these
6 nanoparticles have opened up exciting avenues in a broad range of biomedical applications,
7 including targeted drug delivery.²⁻⁵ For the continued development of nanoparticle-based
8
9
10
11
12
13
14
15
16
17
18
19
20
21
22
23
24
25
26
27
28
29
30
31
32
33
34
35
36
37
38
39
40
41
42
43
44
45
46
47
48
49
50
51
52
53
54
55
56
57
58
59
60

Advances in engineering functional structures at the nanoscale have led to the generation of a wide range of nanoparticles, including silica (SiO₂) nanoparticles, gold nanoparticles, and polymeric nanoparticles.¹ With their dimension in the size ranging from 1 – 100 nm, these nanoparticles have opened up exciting avenues in a broad range of biomedical applications, including targeted drug delivery.²⁻⁵ For the continued development of nanoparticle-based biomedicine, an understanding of the complex interactions between nanoparticles and biological systems is essential.

It is now widely acknowledged that nanoparticles adsorb many biomolecules (mainly proteins) upon exposure to biological milieu, resulting in the formation of a new interface termed the “protein corona”.⁶⁻¹⁴ Increasing evidence has shown that the protein corona regulates nanoparticle-cell recognition, and hence plays important roles in modulating nanoparticle mobility and toxicity.¹⁵⁻²⁰ For example, the adsorption of proteins on nanoparticles has been shown to reduce nanoparticle cell membrane adhesion, mitigating the disruption of cell membranes by bare nanoparticles.²¹ Alternatively, the adsorbed proteins have been shown to negatively impact on the specificity of nanoparticles to targeted cells, resulting in the loss or reduction of the targeting capability of surface functionalized nanoparticles.²² In addition, nanoparticles can induce conformational changes in the adsorbed proteins, which in turn trigger *de novo* nanoparticle-cell recognition and initiate alternative cell signal transduction.²³⁻²⁵ Collectively, the biological relevance of a protein corona is intimately linked with its molecular properties. These molecular details not only include the macroscopic composition of the adsorbed proteins, but also their structure, conformation and organization.

One of the most abundant post-translational modifications of proteins is glycosylation. It is estimated that over 50% of all human proteins are glycosylated.²⁶ In eukaryotic cells most

1
2
3 glycosylation events occur in the endoplasmic reticulum along the (ER)-Golgi-plasma membrane
4 trafficking pathway catalyzed by a series of glycosidases and glycotransferases. In general the
5 attached glycans play a critical role in maintaining protein stability and conformation, facilitating
6 protein folding and trafficking, as well as regulating protein immunogenicity and protein-protein
7 interactions.^{27, 28} Despite the ubiquitous presence of glycans in proteins, little is known about the
8 organization of the glycans in the nanoparticle protein corona and their effects on nanoparticle-
9 cell interactions.
10
11
12
13
14
15
16
17
18
19

20 Herein, we investigate the roles of glycans at the outermost surface of the hard corona in
21 mediating nanoparticle-cell interactions using a model nanoparticle system (SiO₂ nanoparticles).
22 A protein corona derived from human plasma has been chosen for the model corona, as most
23 proteins in the blood plasma are heavily glycosylated, and intravenous administration of
24 nanoparticles is one of the most relevant delivery routes for many biological applications. We
25 incubated SiO₂ nanoparticles with complete human plasma to obtain the hard corona-
26 nanoparticles. Subsequently, the nanoparticles coated with the hard corona are enzymatically
27 deglycosylated *in situ* (Scheme 1). The deglycosylation results in an increase in the
28 electrophoretic mobility of corona proteins observed by sodium dodecyl sulfate polyacrylamide
29 gel electrophoresis (SDS-PAGE). Additionally, fluorescently labeled lectins have been used to
30 monitor the loss of the glycans and to probe the remaining glycan structures on the corona. These
31 studies have revealed that deglycosylation *in situ* partially removes glycans from the corona
32 (even with extended incubation), leading to presentation of new internal glycan structures.
33 Finally, cell membrane adhesion, uptake and cytokine stimulation of the deglycosylated
34 nanoparticle-protein complexes has been evaluated using THP-1 differentiated macrophages.
35
36
37
38
39
40
41
42
43
44
45
46
47
48
49
50
51
52
53
54
55
56
57
58
59
60

1
2
3 Our data show that in comparison to the full corona, the deglycosylation of corona proteins
4 enhances nanoparticle-cell adhesion and stimulates pro-inflammatory responses by macrophages.
5
6
7
8
9

10 RESULTS AND DISCUSSION

11
12
13
14 Fluorescently labeled SiO₂ nanoparticles of 56 nm diameter, as measured by transmission
15 electron microscopy (TEM) (Figure S1), were incubated with human plasma to form a protein
16 corona. The particle size, polydispersity, and zeta-potential were determined by dynamic light
17 scattering (DLS), differential centrifugal sedimentation (DCS), and microelectrophoresis,
18 respectively. The DLS data showed that the adsorption of proteins resulted in an increase of the
19 nanoparticle size (Figure 1a and Table S1), and a change in correlogram and cumulation fit of
20 DLS measurements (Figure S2), which has consistently been seen with other nanoparticles.^{21,29}
21
22
23 In good agreement, DCS measurements exhibited a change in sedimentation time due to the
24 corona formation (Figure S5a). The zeta-potential of the nanoparticles decreased from -18 to -10
25 mV upon the formation of the protein corona (Figure 1b and Table S1). Such neutralization
26 effects of the protein corona on particle surface charge have been observed in both negatively
27 and positively charged nanoparticles,^{29,30} as electrostatic interaction between nanoparticles and
28 proteins is one of the main forces driving the formation of the protein corona,⁶ where colloidal
29 stability is nevertheless maintained through steric stabilization effects during the protein
30 adsorption.
31
32
33
34
35
36
37
38
39
40
41
42
43
44
45
46
47
48

49 To obtain a set of nanoparticle-protein complexes with various degrees of glycosylation, the
50 corona-nanoparticles were treated with a glycosidase mixture (comprising PNGase F, O-
51 glycosidase, neuraminidase, β 1-4 galactosidase, and β -N-acetylglucosaminidase) for different
52 time intervals, removing both N-linked and O-linked glycans at the outermost surface of the
53
54
55
56
57
58
59
60

1
2
3 complexes. For comparison, equivalent corona-nanoparticles were exposed to the same
4 deglycosylation reaction conditions in the absence of glycosidases. Using the cumulant fitting
5 method for DLS, polydispersity index (PDI) was used to quantify relative distribution width. It
6 was shown that the deglycosylation led to a slight increase in the polydispersity of the
7 nanoparticle-protein complexes (Figure 1b and Table S1). The cumulation fits and correlograms
8 of the DLS measurements were further analyzed using a method described previously³¹ (Figure
9 S3-4). It was shown that exposure of the nanoparticles with deglycosylation enzymes resulted in
10 a significant and progressive change in the nanoparticle diffusion due to the loss of glycans
11 (Figure S3). In contrast, exposure of the NP protein corona complexes over time in the same
12 buffer without the glycosidases did not result in any significant changes in diffusion properties,
13 suggesting that these complexes are stable over time (Figure S4). Furthermore, DCS
14 measurements demonstrated that a progressive shift in apparent diameter occurred when the
15 nanoparticle-protein corona complexes were exposed for increasing amount of time to
16 glycosidases (Figure S5b), whereas the control samples (in the absence of glycosidases)
17 remained unchanged (Figure S5c). Combined, these results have suggested that the colloidal
18 stability of the glycosylated and deglycosylated nanoparticle-protein complexes is well
19 maintained throughout the experimental conditions. In addition, all of the nanoparticle-protein
20 complexes exhibited a similar neutral zeta-potential of approximately -10 mV at pH 7.4 and the
21 deglycosylation did not result in significant alterations in their zeta-potential (Figure 1c). Taken
22 together, these data suggest that steric stabilization is one of the main driving forces for the
23 colloidal stability of the nanoparticle-protein complexes. The loss of glycans at the outermost
24 surface of the protein corona results in attenuation of the steric stabilization, leading to a
25 decrease of the overall stability of the nanoparticle-protein complexes.
26
27
28
29
30
31
32
33
34
35
36
37
38
39
40
41
42
43
44
45
46
47
48
49
50
51
52
53
54
55
56
57
58
59
60

1
2
3 To confirm that the enzymatic deglycosylation of the protein corona had indeed occurred *in*
4 *situ*, the proteins from the hard corona were subsequently eluted from the nanoparticles and
5 separated by SDS-PAGE. It was expected that deglycosylated proteins would increase their
6 electrophoretic mobility relative to their fully glycosylated forms. Direct comparison between the
7 enzyme-treated and non-enzyme controls revealed several reproducible differences in the range
8 between 62 – 14 kDa (indicated by arrows in Figure 2). In particular, the proteins near the 28 and
9 14 kDa bands appeared to undergo subtle progressive changes with an increase in the
10 deglycosylation reaction time (Figure 2), suggesting that different degrees of glycosylation
11 remained in the nanoparticle-protein complexes. Extending the incubation time or increasing the
12 concentrations of the deglycosylation enzymes did not lead to further reduction of the apparent
13 molecular weight of the corona proteins on the SDS-PAGE (Figure S7).
14
15
16
17
18
19
20
21
22
23
24
25
26
27
28

29 To identify the proteins that underwent deglycosylation, the deglycosylated and control
30 coronas after enzymatic reaction *in situ* for 120 min were separated by SDS-PAGE. Based on the
31 change of electrophoretic mobility, 6 regions from the lanes of control and deglycosylated
32 coronas were excised from the SDS-PAGE. The proteins were extracted by in-gel tryptic
33 digestion and identified using Electrospray Liquid Chromatography Mass Spectrometry (LC-
34 MS/MS) equipped with a HPLC and an LTQ Orbitrap. The criteria for identification of
35 deglycosylated proteins were set as following: 1) present in both control and deglycosylated
36 coronas; 2) shown the most significant hits ($NpSpc > 1$); and 3) in the molecular weight ranges
37 shown on the SDS-PAGE. A total of 20 deglycosylated proteins were identified, and the type of
38 their glycosylation was estimated (Table 1).
39
40
41
42
43
44
45
46
47
48
49
50
51
52

53 Next, we sought to examine the structure of glycans in the protein corona. Due to their
54 remarkable diversity and complexity, it is challenging and laborious to fully reveal the detailed
55
56
57
58
59
60

1
2
3 glycan structures. The structure elucidation of even simple glycans requires highly sophisticated
4 technical expertise and instrumentation. Thus, here we employed glycan-binding lectins to probe
5 specific glycan structures in the protein corona. Generally, two major forms of glycosylation are
6 present in human plasma proteins, N-linked and O-linked glycosylation (Scheme 2).³² N-glycans
7 are covalently linked to asparagine residues of proteins, whereas O-glycans are conjugated to
8 serine or threonine.²⁸ Generally, N-glycosylation starts from a mannose-rich core structure, and
9 subsequently undergoes a series of adding, trimming and branching monosaccharides, such as
10 galactose (Gal) and *N*-acetylneuraminic acid (Neu5AC), to create N-glycan structures. Similarly,
11 O-glycosylation involves sequential addition of monosaccharides catalyzed by various
12 glycosyltransferases. In this study, three different fluorescently labeled lectins (wheat germ
13 agglutinin (WGA), peanut agglutinin (PNA), and concanavalin A (Con A)) were chosen to probe
14 the glycans structures. Although these lectins have a broad specificity, WGA selectively
15 recognizes Neu5AC, PNA binds to Gal, and Con A associates with mannose (Scheme 2). The
16 deglycosylated and control nanoparticle-protein complexes were incubated with the lectins
17 individually and subsequently the lectin binding was measured as the mean fluorescence
18 intensity by flow cytometry. The nanoparticle-protein complexes post incubation with lectins
19 were analyzed by DCS to ensure that the lectins did not induce nanoparticle aggregation under
20 these conditions (Figure S2). In comparison with nanoparticles coated with bovine serum
21 albumin, which serves as a non-glycosylated control,³³ the full plasma corona showed binding
22 only to WGA (Figure 3). This suggests that Neu5AC is exposed on the corona surface, whereas
23 Gal or mannose is not presented. Upon deglycosylation, the nanoparticle-protein complexes
24 showed a significant decrease of WGA fluorescence intensity (Figure 3a), suggesting rapid
25 removal of the surface Neu5AC monosaccharides even after 15 min of enzymatic reaction.
26
27
28
29
30
31
32
33
34
35
36
37
38
39
40
41
42
43
44
45
46
47
48
49
50
51
52
53
54
55
56
57
58
59
60

1
2
3
4
5
6
7
8
9
10
11
12
13
14
15
16
17
18
19
20
21
22
23
24
25
26
27
28
29
30
31
32
33
34
35
36
37
38
39
40
41
42
43
44
45
46
47
48
49
50
51
52
53
54
55
56
57
58
59
60

Conversely, the deglycosylation of the corona following 120 min incubation led to increased binding to PNA, while by contrast deglycosylation at shorter time intervals (15, 30 and 60 min) did not significantly increase the PNA binding (Figure 3b). The increased binding to PNA after an extended deglycosylation time suggests that Gal monosaccharides are gradually exposed on the corona surface with the loss of outermost glycans. It is also noted that the deglycosylated coronas did not exhibit any significant difference in Con A binding affinity compared with the non-enzymatic controls (Figure 3c), suggesting that mannose is not accessible following the deglycosylation procedure used in this study. Taken together, the lectin binding profile, coupled with the SDS-PAGE data (Figure 2), indicates that the surface glycans on the protein corona undergo progressive removal upon enzymatic deglycosylation *in situ*, which leads to exposure of internal glycans that are not available on the surface of the full corona.

Glycosylation plays an important role in regulating immunity. Alterations of attached glycans can both positively and negatively modulate a number of immune pathways.³⁴ In the context of serum proteins, a well-known example is that of immunoglobulin G (IgG) glycovariants that exhibit different binding affinities for Fc γ receptors (Fc γ Rs) to modulate pro- and anti-inflammatory IgG functionality. For example, sialylation-rich IgG, which has a decreased affinity for the classical Fc γ Rs, promotes an anti-inflammatory milieu,³⁵ whereas IgG bearing a bisecting N-acetylglucosamine (GlcNAc) with an increased affinity for Fc γ RIII accelerates the development of collagen-induced arthritis.³⁶ To evaluate the roles of the surface glycans in nanoparticle-immune cell interactions, we differentiated and polarized monocytic THP-1 cells into pro-inflammatory M1 and anti-inflammatory M2 macrophages using an established protocol described previously to represent two major and opposing macrophage functionalities.³⁶ Briefly, the M1 phenotype is induced by pro-inflammatory milieu (*e.g.*, interferon- γ). In contrast,

1
2
3 polarization to M2 macrophages often involves interleukin-4.³⁷ In general M1 macrophages
4 mount potent microbicidal immune responses, whereas M2 macrophages play important roles in
5 homeostasis and tissue repairing.³⁷ The deglycosylated nanoparticle-protein complexes were
6 dispersed in serum free medium and incubated with M1- or M2-macrophages at 4 °C for 1 h to
7 allow binding to the cell membrane without internalization. In the case of M1-macrophages, the
8 nanoparticle-protein complexes with shorter deglycosylation reaction times (15, 30 and 60 min)
9 did not show significant difference in cell membrane adhesion compared with the non-enzyme
10 controls (Figure 4a). However, the further loss of glycans (deglycosylation for 120 min) resulted
11 in an increase of cell membrane adhesion (Figure 4a). Consistently, the deglycosylation of the
12 protein corona led to an enhanced cell membrane adhesion to the M2-macrophages (Figure 4b).
13
14 Several possible underlying mechanisms can play a role in the increased adhesion of the
15 deglycosylated nanoparticle-protein complexes on the cell membrane. The removal of glycans on
16 the surface of the protein corona potentially has pleiotropic effects. First, the loss of glycans can
17 reduce the steric repulsion between the corona-nanoparticles and the macrophage cell membrane,
18 increasing non-specific interactions. Second, it can expose underlying glycans or new epitopes,
19 which in turn induces specific interactions with receptors that recognize modified endogenous
20 molecules (*e.g.*, scavenger receptors) in macrophages. It is also noted that M2-macrophages
21 appeared to be more sensitive to the loss of the glycans compared with M1-macrophages, as the
22 partial removal of glycans after the deglycosylation reaction for 30 min already significantly
23 increased the adhesion to M2-macrophage membrane. The distinct cell membrane properties
24 between M1- and M2-macrophages can be one of the possibilities for their difference in the
25 sensitivity to glycans. It is well known that M1-macrophages express high levels of FcγRI,
26 whereas M2-macrophages express abundant amounts of mannose receptor and scavenger
27
28
29
30
31
32
33
34
35
36
37
38
39
40
41
42
43
44
45
46
47
48
49
50
51
52
53
54
55
56
57
58
59
60

1
2
3 receptor CD163.³⁷ Such molecular traits are likely to define the extent of the enhanced non-
4
5 specific and/or specific interactions occurring between the nanoparticle-protein complexes and
6
7 the cell membrane.
8
9

10 In general, elevated cell membrane adhesion is expected to facilitate cell membrane wrapping,
11 leading to an increase in cell uptake of nanoparticles.⁶ To evaluate the effect of glycans in the
12 protein corona on cell uptake, the nanoparticle-protein complexes were incubated with M1- or
13 M2-macrophages at 37 °C in serum free media for various time intervals. For these studies, the
14 nanoparticle-protein complexes that were deglycosylated for 120 min were chosen, as they
15 resulted in enhanced cell membrane adhesion in both M1- and M2-macrophages. The full
16 glycosylated and deglycosylated protein coronas post incubation with serum free media were
17 analyzed by SDS-PAGE to ensure that desorption of the proteins was minimal under the
18 conditions (Figure S8). The extent of uptake was measured by the mean fluorescence intensity of
19 cells as a function of time over 5 h in serum free medium. The flow cytometry data showed
20 essentially linear uptake kinetics for all the different nanoparticle-protein complexes (Figure 5).
21 Importantly, the deglycosylated nanoparticle-protein complexes exhibited a higher uptake both
22 in M1- and M2-macrophages at all time intervals (Figure 5), which is consistent with the
23 observation of enhanced cell membrane adhesion. It is also noted that under the same treatment
24 conditions, M2-macrophages showed a higher mean fluorescence intensity than M1-
25 macrophages, suggesting that more nanoparticles were internalized by M2-macrophages (Figure
26 5). Studies have shown that the effect of macrophage polarization on phagocytosis is dependent
27 on targets. In comparison to M1 macrophages, M2 macrophages show greater phagocytosis of
28 myelin,³⁸ apoptotic cells,³⁹ latex beads,³⁹ and dextran.⁴⁰ A future study on the direct comparison
29 of gene expression profiles between M1 and M2 macrophages, in particular key molecules
30
31
32
33
34
35
36
37
38
39
40
41
42
43
44
45
46
47
48
49
50
51
52
53
54
55
56
57
58
59
60

1
2
3 involved in phagocytosis, is likely to shed light on the higher endocytic capability of the
4
5
6 nanoparticle-protein complexes in M2 macrophages.
7

8
9
10
11
12
13
14
15
16
17
18
19
20
21
22
23
24
25
26
27
28
29
30
31
32
33
34
35
36
37
38
39
40
41
42
43
44
45
46
47
48
49
50
51
52
53
54
55
56
57
58
59
60

Next, we sought to investigate potential pro- or anti-inflammatory effects of macrophages in relation to nanoparticle internalization. The serum free media were collected after incubation of the nanoparticle-protein complexes with M1- or M2-macrophages at 37 °C for 5 h. Production of pro-inflammatory cytokines – human interleukin-1 β (hIL-1 β) and human tumor necrosis factor- α (hTNF- α), as well as an anti-inflammatory cytokine human transforming growth factor- β 1 (hTGF- β 1) – was measured in culture medium by an enzyme-linked immunosorbent assay (ELISA). As expected, M1 macrophages were found to express significantly higher levels of hIL-1 β and hTNF- α in comparison to M2 macrophages (Figure 6). In M1 macrophages, the uptake of nanoparticle-protein complexes (including both glycosylated and deglycosylated corona-nanoparticles) led to an increase of hIL-1 β and hTNF- α , but a reduction of hTGF- β 1 (Figure 6a-c). Compared with the fully glycosylated nanoparticle-protein complexes (referred to as M1+E- in Figure 6), deglycosylation of the protein corona resulted in a further increase of hIL-1 β and a decrease of hTGF- β 1 in M1 macrophages (Figure 6a and c), suggesting that deglycosylated nanoparticle-protein complexes promote a pro-inflammatory milieu. Consistently, the pro-inflammatory cytokine hTNF- α was elevated in M2 macrophages after exposure to deglycosylated corona-nanoparticles (Figure 6e) compared with the full corona-nanoparticles. The pro-inflammatory properties of nanoparticles have been reported previously due to various underlying mechanisms, including oxidative stress,⁴¹ activation of Mac-1 pathway,²³ and recognition by scavenger receptors.²⁵ Detailed analysis of the molecular mechanisms for the up-regulation of pro-inflammatory cytokines and down-regulation of anti-

1
2
3 inflammatory cytokine after exposure to deglycosylated nanoparticle-protein complexes remain a
4
5 subject of future investigations.
6
7
8
9

10 CONCLUSIONS

11
12 Glycosylation is one of the most frequent post-translational modifications of proteins, and
13 confers a diversity of structural and functional properties. The present study provides the first
14 investigation on the impact of glycosylation of a protein corona on the physicochemical
15 properties of nanoparticles and their cellular interactions. Firstly, a series of deglycosylated
16 protein coronas on SiO₂ nanoparticles were obtained by enzymatic deglycosylation *in situ* of the
17 hard corona-nanoparticles. A progressive loss of the outermost surface glycans of the protein
18 corona was characterized by SDS-PAGE and profiled by lectin binding. Our data show that the
19 *in situ* deglycosylation leads to partial removal of the glycans in the protein corona, which
20 decreases the colloidal stability of nanoparticle-protein complexes. The resulting deglycosylated
21 nanoparticle-protein complexes have been shown to enhance cell membrane adhesion to two
22 types of THP-1 differentiated macrophages (polarized to M1 and M2), leading to an increase in
23 nanoparticle uptake. Further, the deglycosylated corona-nanoparticles exhibit pro-inflammatory
24 properties compared with the fully glycosylated form, suggesting the importance of
25 glycosylation in the immunological interactions of nanoparticles. It is also worth noting that the
26 formation of protein coronas is strongly influenced by nanoparticle size and surface chemistry.²⁹
27 Hence, the degree of glycosylation of protein coronas and the effect of cellular interactions may
28 vary depending on physicochemical properties of nanoparticles. To fully elucidate the roles of
29 glycans in a protein corona with respect to nanoparticle-cell recognition, receptor activation, and
30 signal transduction, future studies will be aimed at characterizing the glycan repertoire of a given
31
32
33
34
35
36
37
38
39
40
41
42
43
44
45
46
47
48
49
50
51
52
53
54
55
56
57
58
59
60

1
2
3 corona. Moreover, since proteins undergo a variety of post-translational modifications (*e.g.*
4 phosphorylation, acetylation, and methylation), this study exemplifies how such covalent
5 addition to proteins can have biological significance for the nanoparticle protein corona,
6 increasing their diversity and complexity.
7
8
9
10
11

12 13 14 15 METHODS

16
17 **Materials:** Tetraethyl orthosilicate (TEOS), 3-Aminopropyl trimethoxysilane, Fluorescein
18 Isothiocyanate (Isomer I) (FITC), L-Arginine and IGEPAL CO-520 were all purchased from
19 Sigma-Aldrich and used as received. Commercially sourced SiO₂ nanoparticles were purchased
20 from Kisker (Steinfurt, Germany). Roswell Park Memorial Institute 1640 containing GlutaMax
21 (RPMI), heat-inactivated fetal bovine serum (HI-FBS), Phosphate-Buffered Saline (PBS),
22 NuPAGE Bis-Tris Precast Gel 4-12%, NuPAGE MES SDS Running Buffer, NuPAGE LDS
23 Sample Buffer, NuPAGE Sample Reducing Agent, SeeBlue Plus2 Pre-stained Protein Standard,
24 SimpleBlue SafeStain, IL-1 β , TNF- α , and TGF- β human ELISA kits, AF633-wheat germ
25 agglutinin (AF633-WGA), AF633-concanavalin A (AF633-Con A), and AF647-peanut
26 agglutinin (AF647-PNA) were purchased from Life Technologies. Interleukin-4 (IL-4),
27 interleukin-13 (IL-13), lipopolysaccharide (LPS), and interferon- γ (IFN- γ) were purchased from
28 Invivogen. Phorbol 12-myristate 13-acetate (PMA) were purchased from Sigma-Aldrich. Human
29 plasma was purchased from BioreclamationIVT. Ultrapure water with resistance greater than 18
30 M Ω cm was obtained from an inline Millipore RiOs/Origin system (Millipore Corporation,
31 USA).
32
33
34
35
36
37
38
39
40
41
42
43
44
45
46
47
48
49
50

51
52 **FITC conjugate:** N-1-(3-trimethoxysilylpropyl)-N'-fluoresceyl thiourea (FITC-APTMS)
53 conjugate solution was prepared by dissolving 2 mg of FITC in 2 ml of anhydrous ethanol. 10 μ l
54 of APTMS (11 \times molar excess) was then added immediately to this solution and the mixture then
55
56
57
58
59
60

1
2
3 shaken at room temperature in the dark for 4 h. This reaction was monitored by ^1H NMR
4
5 (CD₃OD) where a shift in the signal from the proton adjacent to the amine group
6
7 (Si(OCH₃)₃CH₂CH₂CH₂NH₂) upon coupling FITC reached an integration value constant and
8
9 equal to the aromatic FITC signal. The reaction was deemed complete at 4 h.
10
11

12 **SiO₂ Nanoparticle Syntheses:** Fluorescent SiO₂ nanoparticles (56 nm) were prepared as
13
14 follows. SiO₂ nanoparticles (5.9 g) were added to aqueous ammonia (28 % w/w) and supplied
15
16 with methanol to a total volume of 50 mL while rapidly stirred. 1 mL of the FITC conjugate
17
18 solution was then added to this mixture followed 1 min later by 1.9 mL of TEOS. The reaction
19
20 was sealed and stirred at 40 °C for a further 3 h. The particles were washed three times by
21
22 centrifugation at 14 000 g for 20 min with resuspension in ethanol and water using bath
23
24 sonication (Branson 1510) for each washing cycle. The resulting pellet was resuspended in water
25
26 to give a final volume of 25 mL. Mass concentration was measured following vacuum drying at
27
28 600 °C for 12 h.
29
30
31
32
33

34 **Preparation of Hard Protein Corona of SiO₂ Nanoparticles:** Nanoparticles (30 μL,
35
36 concentration 17 mg mL⁻¹) were incubated with human plasma (470 μL) at 37 °C for 1 h with
37
38 continuous agitation. After incubation, the nanoparticles-protein complex was pelleted from
39
40 excess plasma by centrifugation at 18 000 g, 4 °C for 20 min. The supernatant was discarded and
41
42 the pellet was then re-suspend in 500 μL PBS and centrifuged again to pellet nanoparticles-
43
44 protein complex. The washing procedure removes unbound and loosely bound proteins from
45
46 nanoparticles. The hard corona-nanoparticles are obtained after repeating the washing step three
47
48 times.
49
50
51
52

53 **Deglycosylation of SiO₂ Nanoparticle Protein Corona:** Deglycosylation of the protein
54
55 coronas was performed *in situ* using Protein Deglycosylation Mix (New England Biolabs) as per
56
57
58
59
60

1
2
3 the manufacturer's instructions. Briefly, approximate 500 μg SiO_2 nanoparticle-protein
4 complexes in were suspended in 50 μL reaction buffer containing 1 μL of Deglycosylation
5 Enzyme Mix. The reaction mixture was incubated at 37 $^\circ\text{C}$ for various time periods. After the
6
7
8
9
10
11
12
13
14
15
16
17
18
19
20
21
22
23
24
25
26
27
28
29
30
31
32
33
34
35
36
37
38
39
40
41
42
43
44
45
46
47
48
49
50
51
52
53
54
55
56
57
58
59
60

the manufacturer's instructions. Briefly, approximate 500 μg SiO_2 nanoparticle-protein complexes in were suspended in 50 μL reaction buffer containing 1 μL of Deglycosylation Enzyme Mix. The reaction mixture was incubated at 37 $^\circ\text{C}$ for various time periods. After the reaction, the samples were immediately replaced on ice to slow down the reaction, and centrifuged at 18 000 g, 4 $^\circ\text{C}$ for 20 min. The supernatant was discarded, and the nanoparticles were resuspended in PBS.

Dynamic Light Scattering: SiO_2 nanoparticle-protein complexes (250 $\mu\text{g mL}^{-1}$) were suspended in PBS at pH 7.4 and measured with Malvern PCS-4700 instrument equipped with a 256-channel correlator. The zeta potential determination was performed using a Malvern Zetasizer 3000HSa.

SDS-PAGE: The protein coronas on the nanoparticles (10 μL , concentration of 12.5 g L^{-1}) following deglycosylation were eluted by mixing with NuPAGE LDS sample buffer and NuPAGE sample reducing agent, and heating at 70 $^\circ\text{C}$ for 10 min as per the manufacturer's instructions. The samples were then centrifuged at 18 000 g, 4 $^\circ\text{C}$ for 20 min. The supernatant was then loaded into NuPAGE Bis-Tris precast gel 4-12%. The proteins were separated by gel electrophoresis in NuPAGE MES SDS Running Buffer. The gel was stained with SimplyBlue SafeStain as per the manufacturer's instructions (Life Technologies).

Identification of deglycosylated proteins by mass spectrometry: To determine the deglycosylated proteins, the gel bands with and without enzymatic treatment for deglycosylation were cut out following SDS-PAGE. The gel digestion was performed as per the described method from Shevchenko et al.⁴² The digested peptides were then re-suspended in 0.1% formic acid. Electrospray Liquid Chromatography Mass Spectrometry (LC-MS/MS) equipped with a HPLC (Surveyor, ThermoFinnigan, CA) and interfaced with an LTQ Orbitrap (ThermoFinnigan,

1
2
3 CA) was used to analyze peptide mixtures following trypsin digestion. Spectra were searched
4
5 with Peaks 7 software (Bioinformatics Solutions Inc) using Sequest Uniprot/Swiss-Prot database
6
7 (www.expasy.org). The spectral count of each protein was then converted into a Normalized
8
9 Spectral Count (NSpC), which was calculated using the spectral counting method as the
10
11 following equation²⁹: [ref]:
12
13

$$14 \quad NpSpC_k = \left(\frac{(SpC/M_w)_k}{\sum_{i=1}^n (SpC/M_w)_i} \right) \times 100$$

15
16
17
18
19
20
21 Where $NpSpC_k$ is the percentage of the normalised spectral count for protein k , SpC is the
22
23 spectral count, and M_w is the molecular weight (KDa) of protein k .
24
25

26 **Lectin Binding:** SiO₂ nanoparticle-protein complexes (1 mg mL⁻¹ nanoparticles) were
27
28 incubated with AF633-WGA, AF633-ConA, or AF647-PNA at a final concentration of 10 μg
29
30 mL⁻¹ at 25 °C for 30 min. After the incubation, the reaction mixture was immediately centrifuged
31
32 at 18 000 g, 4 °C for 20 min to remove excess lectin from the solution. The supernatant was
33
34 discarded, and the nanoparticles were resuspended in PBS. The fluorescence intensity of the
35
36 nanoparticles was analyzed by flow cytometry (Accuri, BD). Results are presented as the mean
37
38 fluorescence intensity of nanoparticles from triplicates measuring at least 100 000 particles for
39
40 each replicate.
41
42
43
44

45 **Cell Culture:** Human monocytic leukemia cell line THP-1 (American Type Culture
46
47 Collection) cells were maintained in RPMI media with the addition of 10% (v/v) HI-FBS at 37
48
49 °C in a 5% CO₂ humidified atmosphere. M1 and M2 macrophages were generated as described
50
51 previously.³⁶ Briefly, THP-1 cells were firstly differentiated into macrophages with 320 nM
52
53 PMA for 6 h, and subsequently polarized with 320 nM PMA, 100ng mL⁻¹ LPS, and 20 ng mL⁻¹
54
55 IFN-γ for 18 h to generate M1 macrophages. To obtain M2 macrophages, THP-1 cells were
56
57
58
59
60

1
2
3 treated with 320 nM PMA for 6 h, and then cultured with 320 nM PMA, 20 ng mL⁻¹ IL-4 and
4
5 20 ng mL⁻¹ IL-13 for 18 h.
6
7

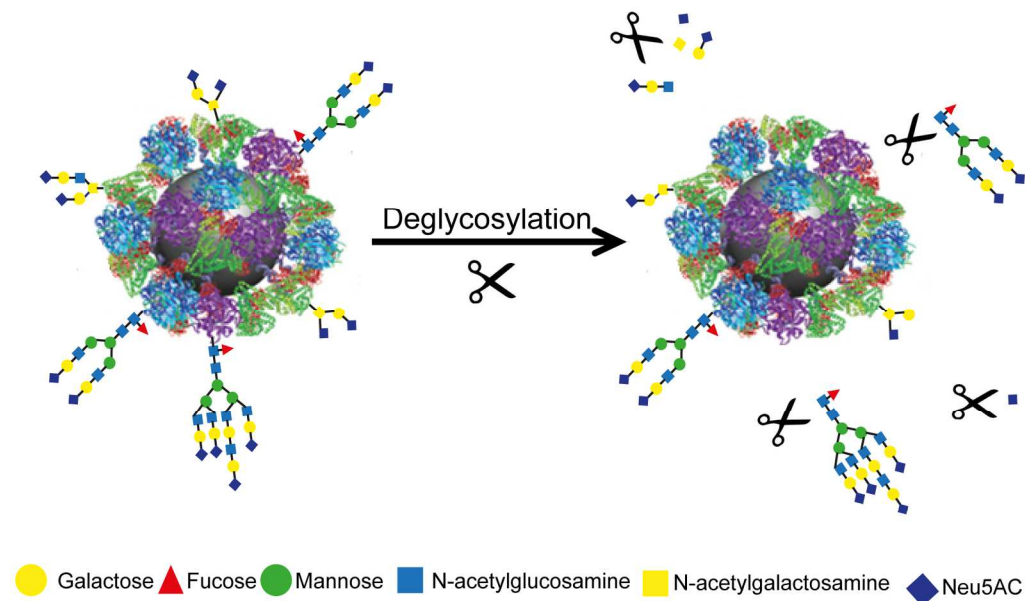
8 **Cell Membrane Adhesion of Nanoparticles by Flow Cytometry:** THP-1 cells were
9
10 differentiated and polarized at a density of 1×10^5 cells in 0.5 mL complete growth media into
11
12 24-well plates. After differentiation and polarization, the cells were washed twice with cold PBS,
13
14 and incubated with cold serum free RPMI media containing 100 $\mu\text{g mL}^{-1}$ nanoparticles at 4 °C
15
16 for 1 h. The treatment media were discarded, and the cells were then gently washed with PBS
17
18 twice to remove unbound nanoparticles, resuspended by gentle pipetting in cold PBS, and
19
20 analyzed by flow cytometry (CyFlow Space, Partec GmbH). Results are presented as the mean
21
22 fluorescence intensity of cells from at least 10 000 cells for each replica.
23
24
25
26

27 **Cellular Uptake of Nanoparticles by Flow Cytometry:** THP-1 cells were differentiated
28
29 and polarized at a density of 1×10^5 cells in 0.5 mL complete growth media into 24-well plates.
30
31 After differentiation and polarization, the cells were washed twice with cold PBS, and incubated
32
33 with pre-warmed (37 °C) serum free RPMI media containing 25 $\mu\text{g mL}^{-1}$ nanoparticles at 37 °C,
34
35 5% CO₂ for various time intervals. The treatment media were discarded, and the cells were then
36
37 gently washed with PBS twice to remove unbound nanoparticles, resuspended by gentle
38
39 pipetting in cold PBS, and analyzed by flow cytometry (CyFlow Space, Partec GmbH). Results
40
41 are presented as the mean fluorescence intensity of cells from at least 10 000 cells for each
42
43 replica.
44
45
46
47

48 **Cytokine Assay:** M1 and M2 macrophages were incubated with 25 $\mu\text{g mL}^{-1}$ nanoparticles at
49
50 37 °C, 5% CO₂ for 5 h. The supernatant was collected and centrifuged at 18 000 g at 4 °C for 20
51
52 min to remove any remaining nanoparticles or cell debris. hIL-1 β , hTNF- α , and hTGF- β 1 levels
53
54
55
56
57
58
59
60

1
2
3 in the supernatant were measured by ELISA (Life Technologies) as per the manufacturer's
4
5 instructions.
6
7
8
9
10
11
12
13
14
15
16
17
18
19
20
21
22
23
24
25
26
27
28
29
30
31
32
33
34
35
36
37
38
39
40
41
42
43
44
45
46
47
48
49
50
51
52
53
54
55
56
57
58
59
60

FIGURES



Scheme 1. *In situ* enzymatic deglycosylation of the hard protein corona on nanoparticles. Nanoparticle-protein complexes are treated with a mixture of endoglycosidases and exoglycosidases to remove the outermost surface glycans while the proteins are retained on the nanoparticles.

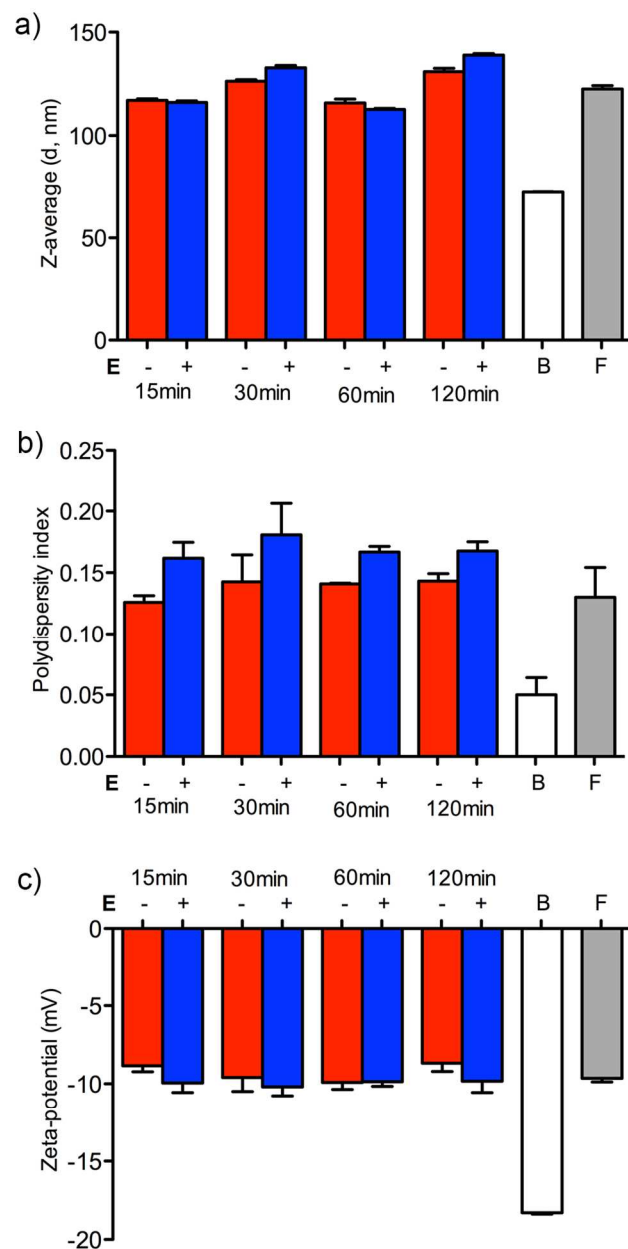


Figure 1. Characterization of SiO₂ nanoparticle-protein complexes before and after deglycosylation: z-average hydrodynamic diameter (a), polydispersity index (b), and zeta-potential (c). Nanoparticle-complexes were deglycosylated *in situ* for various time periods (15 min, 30 min, 60 min, and 120 min, respectively, E+). E- represents non-enzyme-treated controls. Bare nanoparticles and full protein corona-nanoparticles were referred to as B and F,

1
2
3 respectively. Data of z-average and zeta-potential are the mean \pm standard error of three
4
5
6 measurements.
7
8
9
10
11
12
13
14
15
16
17
18
19
20
21
22
23
24
25
26
27
28
29
30
31
32
33
34
35
36
37
38
39
40
41
42
43
44
45
46
47
48
49
50
51
52
53
54
55
56
57
58
59
60

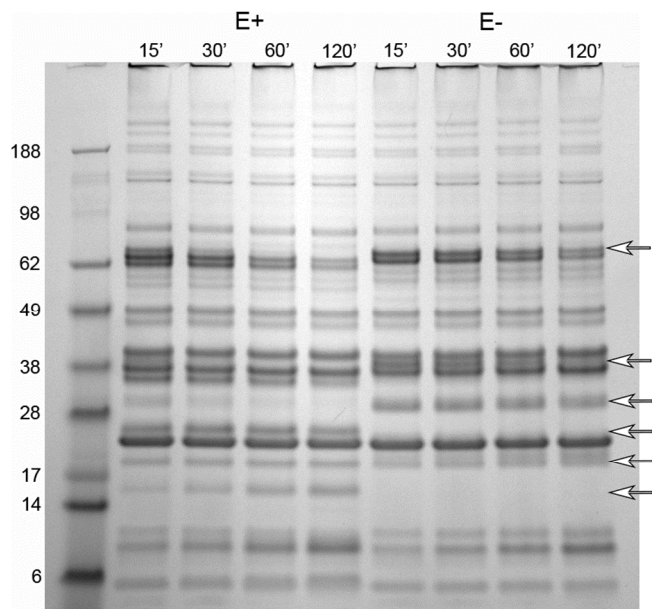
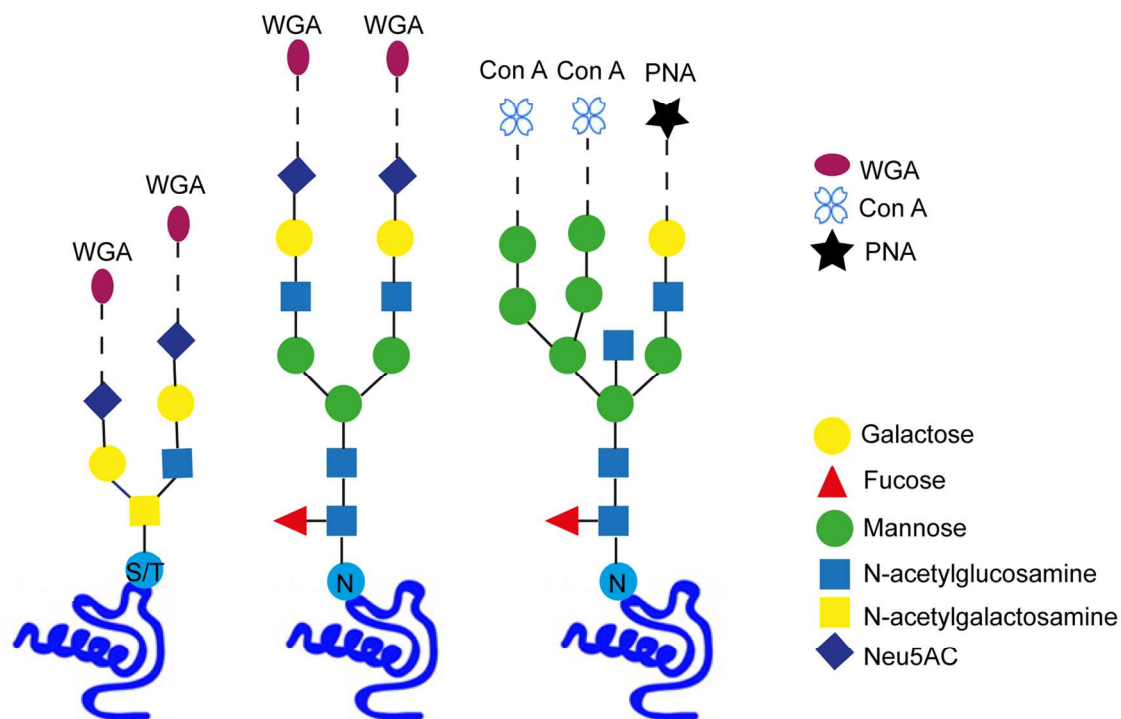


Figure 2. SDS-PAGE of protein coronas recovered from SiO₂ nanoparticles following incubation with human plasma and subsequent enzymatic deglycosylation *in situ* for various time periods (15, 30, 60, and 120 min, respectively, E+). E- represents the equivalent non-enzyme-treated controls. Arrows indicate the bands that have shifted between E- and E+. Molecular weight ladder is shown on the left (unit, kDa).

Table 1. List of the Most Abundant Deglycosylated Proteins Identified by Mass Spectrometry after Enzymatic Deglycosylation Reaction *in situ*

Accession	Mw (Da)	Protein	Glycosylation description
P02671 FIBA	94 973	Fibrinogen alpha chain	N- and O-linked
P00747 PLMN	90 569	Plasminogen	N- and O-linked
P02787 TRFE	77 064	Serotransferrin	N-linked
P01042 KNG1	71 957	Kininogen-1	N- and O-linked
Q9NQ79 CRAC 1	71 421	Cartilage acidic protein 1	O-linked
P00748 FA12	67 792	Coagulation factor XII	N- and O-linked
P04196 HRG	59 578	Histidine-rich glycoprotein	N-linked
P05155 IC1	55 154	Plasma protease C1 inhibitor	N- and O-linked
P04004 VTNC	54 306	Vitronectin	N-linked
P08670 VIME	53 652	Vimentin	O-linked
P01871 IGHM	51 790	Ig mu chain C region	N-linked
P00738 HPT	45 205	Haptoglobin	N-linked
P01876 IGHA1	37 655	Ig alpha-1 chain C region	N- and O-linked
Q03591 FHR1	37 651	Complement factor H-related protein 1	N-linked
P02649 APOE	36 154	Apolipoprotein E	N- and O-linked
P01857 IGHG1	36 106	Ig gamma-1 chain C region	N-linked
Q15485 FCN2	34 001	Ficolin-2	N-linked
O75636 FCN3	32 903	Ficolin-3	N-linked
P02647 APOA1	30 778	Apolipoprotein A-I	N-linked
P05090 APOD	21 276	Apolipoprotein D	N-linked



27
28 **Scheme 2.** O-linked and N-linked glycan structures on human plasma proteins, and the glycan-
29
30 binding specificity of three types of lectins. S/T: Serine or Threonine; N: Asparagine.
31
32
33
34
35
36
37
38
39
40
41
42
43
44
45
46
47
48
49
50
51
52
53
54
55
56
57
58
59
60

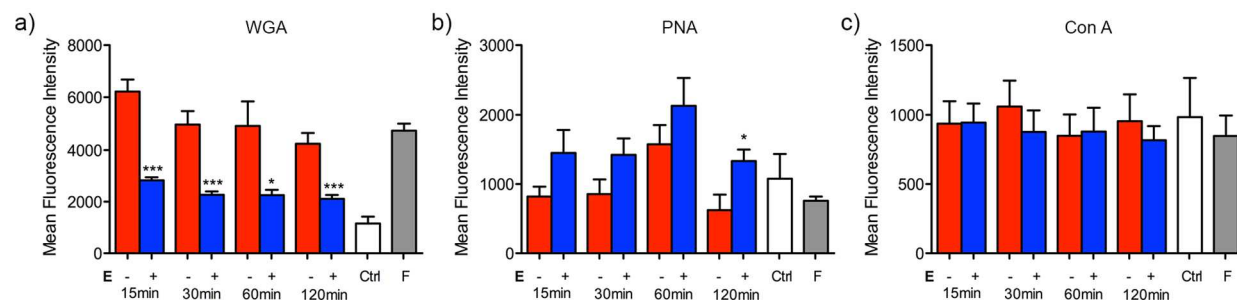


Figure 3. Lectin binding profiles of SiO₂ nanoparticle-protein complexes obtained following deglycosylation for different time periods: WGA (a), PNA (b), and Con A (c). Nanoparticles coated with BSA were used as negative controls (labeled as ctrl), and full protein corona-nanoparticles were referred to as F. Nanoparticle-protein complexes were incubated with fluorescently labeled lectins at 25 °C for 30 min. The mean fluorescence intensity of nanoparticles was measured by flow cytometry. Data are the mean \pm standard error of six independent experiments. * $p < 0.05$, *** $p < 0.001$ (paired t-test between E- and E+).

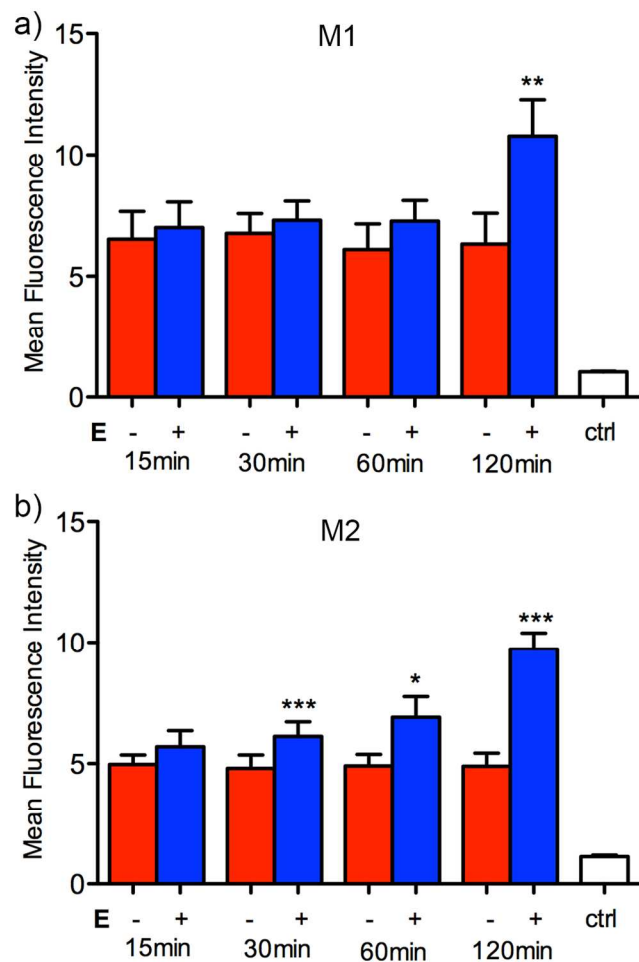


Figure 4. Cell membrane adhesion of fluorescent SiO₂ nanoparticle-protein complexes to M1 (a) and M2 (b) macrophages in serum free media. Nanoparticle-protein complexes were treated with glycosidases for various time periods (15, 30, 60, and 120 min, respectively). E- represents the equivalent non-enzyme-treated controls. Subsequently, cells were incubated with the resulting nanoparticles (100 $\mu\text{g mL}^{-1}$) at 4 °C for 1 h, followed by washing with PBS to remove excess unbound nanoparticles. The mean fluorescence intensity of cells was measured by flow cytometry, and untreated cells were used as controls (labeled as ctrl). Data are the mean \pm standard error of three independent experiments, each performed in duplicate. * $p < 0.05$, ** $p < 0.01$, *** $p < 0.001$ (paired t-test between E- and E+).

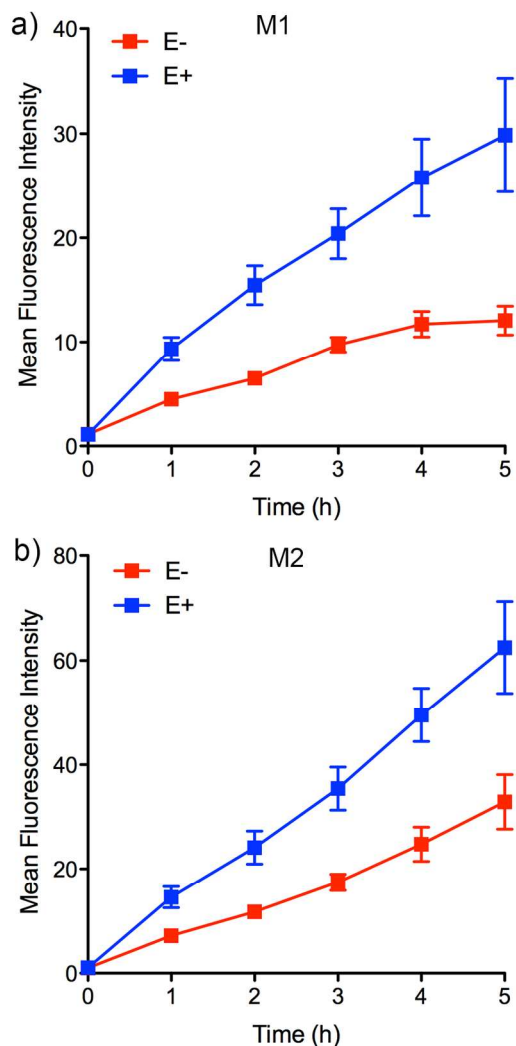


Figure 5. Cell uptake of fluorescent SiO₂ nanoparticle-protein complexes by M1 (a) and M2 (b) macrophages in serum free media. Nanoparticle-protein complexes were treated with glycosidases for 120 min (E+), and the non-enzyme-treated control is shown as E-. Subsequently, cells were incubated with the resulting nanoparticles (25 $\mu\text{g mL}^{-1}$) at 37 $^{\circ}\text{C}$, 5% CO₂ for various time intervals, followed by washing with PBS to remove excess unbound nanoparticles. The mean fluorescence intensity of cells was measured by flow cytometry. Data are the mean \pm standard error of three independent experiments, each performed in duplicate.

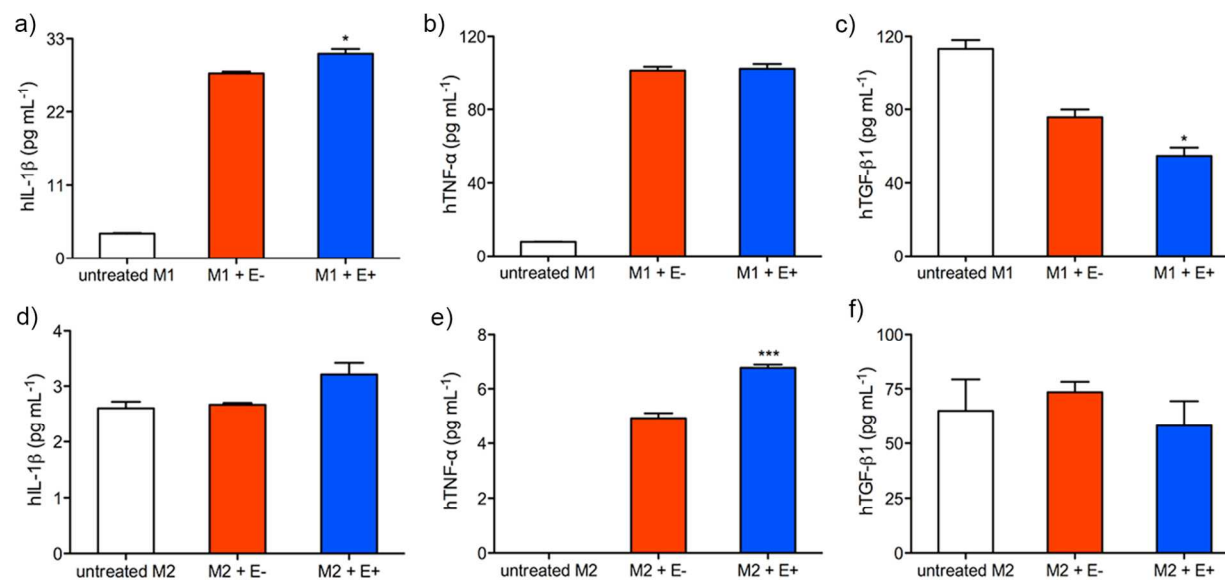


Figure 6. Cytokine expression by M1 (a-c) and M2 (d-f) macrophages. Nanoparticle-protein complexes were treated with glycosidases for 120 min (E+), and the non-enzyme-treated control is shown as E-. Subsequently, cells were incubated with the resulting nanoparticles ($25 \mu\text{g mL}^{-1}$) at 37°C , 5% CO_2 for 5 h. The supernatant was harvested, and cytokines were measured in duplicate. Data are expressed as mean \pm standard error. * $p < 0.05$, *** $p < 0.001$ (unpaired t-test between E- and E+).

1
2
3 ASSOCIATED CONTENT
4
5

6 **Supporting Information.** Table of physiochemical characterization of SiO₂ nanoparticle-
7 protein complexes after deglycosylation. TEM images of SiO₂ nanoparticles. DCS analysis of
8 nanoparticle-protein complexes. SDS-PAGE of protein coronas after enzymatic deglycosylation
9 *in situ* for extended time periods and a higher enzyme concentration. This material is available
10 free of charge *via* the Internet at <http://pubs.acs.org>.
11
12
13
14
15
16
17
18
19

20
21 ACKNOWLEDGMENT
22
23

24 This work was supported by the European Commission under grant agreement of FP7-309329
25 (Nanosolutions), SFI PI Award (12/IA/1422; awarded to K.D.), the Irish Research Council under
26 the EMBARK scheme (RS/2011/106), the Australian Research Council under the Australian
27 Laureate Fellowship (F.C., FL120100030), the Discovery Early Career Researcher Award (Y.Y.,
28 DE130100488), the Australian Research Council Centre of Excellence in Convergent Bio-Nano
29 Science and Technology (CE140100036), and the University of Melbourne under the Dyason
30 Fellowship (Y.Y.).
31
32
33
34
35
36
37
38
39
40
41
42
43
44
45
46
47
48
49
50
51
52
53
54
55
56
57
58
59
60

REFERENCES

1. Albanese, A.; Tang, P. S.; Chan, W. C. The Effect of Nanoparticle Size, Shape, and Surface Chemistry on Biological Systems. *Annu. Rev. Biomed. Eng.* **2012**, *14*, 1-16.
2. Mura, S.; Nicolas, J.; Couvreur, P. Stimuli-Responsive Nanocarriers for Drug Delivery. *Nat. Mater.* **2013**, *12*, 991-1003.
3. Dawidczyk, C.; Russell, L.; Searson, P. C. Nanomedicines for Cancer Therapy: State-Of-The-Art and Limitations to Pre-clinical Studies that Hinder Future Developments. *Front. Chem.* **2014**, *2*, Doi: 10.3389.
4. Pelaz, B.; Charron, G.; Pfeiffer, C.; Zhao, Y.; de la Fuente, J. M.; Liang, X. J.; Parak, W. J.; del Pino, P. Interfacing Engineered Nanoparticles with Biological Systems: Anticipating Adverse Nano-Bio Interactions. *Small* **2013**, *9*, 1573-1584.
5. Malmsten, M. Inorganic Nanomaterials as Delivery Systems for Proteins, Peptides, DNA, and siRNA. *Curr. Opin. Colloid Interface Sci.* **2013**, *18*, 468-480.
6. Walkey, C. D.; Chan, W. C. Understanding and Controlling the Interaction of Nanomaterials with Proteins in A Physiological Environment. *Chem. Soc. Rev.* **2012**, *41*, 2780-2799.
7. Nel, A. E.; Mädler, L.; Velegol, D.; Xia, T.; Hoek, E. M. V.; Somasundaran, P.; Klaessig, F.; Castranova, V.; Thompson, M. Understanding Biophysicochemical Interactions at the Nano-Bio Interface. *Nat. Mater.* **2009**, *8*, 543-557.
8. Cedervall, T.; Lynch, I.; Lindman, S.; Berggård, T.; Thulin, E.; Nilsson, H.; Dawson, K. A.; Linse, S. Understanding the Nanoparticle-Protein Corona Using Methods to Quantify Exchange Rates and Affinities of Proteins for Nanoparticles. *Proc. Natl. Acad. Sci. U. S. A.* **2007**, *104*, 2050-2055.

- 1
2
3
4
5
6
7
8
9
10
11
12
13
14
15
16
17
18
19
20
21
22
23
24
25
26
27
28
29
30
31
32
33
34
35
36
37
38
39
40
41
42
43
44
45
46
47
48
49
50
51
52
53
54
55
56
57
58
59
60
9. Tenzer, S.; Docter, D.; Kuharev, J.; Musyanovych, A.; Fetz, V.; Hecht, R.; Schlenk, F.; Fischer, D.; Kiouptsi, K.; Reinhardt, C.; *et al.* Rapid Formation of Plasma Protein Corona Critically Affects Nanoparticle Pathophysiology. *Nat. Nanotechnol.* **2013**, *8*, 772-781.
 10. Casals, E.; Pfaller, T.; Duschl, A.; Oostingh, G. J.; Puntès, V. F. Hardening of the Nanoparticle-Protein Corona in Metal (Au, Ag) and Oxide (Fe₃O₄, CoO, and CeO₂) Nanoparticles. *Small* **2011**, *7*, 3479-3486.
 11. Dobrovolskaia, M. A.; Patri, A. K.; Zheng, J.; Clogston, J. D.; Ayub, N.; Aggarwal, P.; Neun, B. W.; Hall, J. B.; McNeil, S. E. Interaction of Colloidal Gold Nanoparticles with Human Blood: Effects on Particle Size and Analysis of Plasma Protein Binding Profiles. *Nanomed. Nanotech. Biol. Med.* **2009**, *5*, 106-117.
 12. Liu, W.; Rose, J.; Plantevin, S.; Auffan, M.; Bottero, J.-Y.; Vidaud, C. Protein Corona Formation for Nanomaterials and Proteins of A Similar Size: Hard or Soft Corona? *Nanoscale* **2013**, *5*, 1658-1668.
 13. Scopelliti, P. E.; Borgonovo, A.; Indrieri, M.; Giorgetti, L.; Bongiorno, G.; Carbone, R.; Podesta, A.; Milani, P. The Effect of Surface Nanometre-Scale Morphology on Protein Adsorption. *PLoS One* **2010**, *5*, e11862.
 14. Chanana, M.; Rivera_Gil, P.; Correa-Duarte, M. A.; Liz-Marzán, L. M.; Parak, W. J. Physicochemical Properties of Protein-Coated Gold Nanoparticles in Biological Fluids and Cells before and after Proteolytic Digestion. *Angew. Chem., Int. Ed.* **2013**, *52*, 4179-4183.
 15. Monopoli, M. P.; Åberg, C.; Salvati, A.; Dawson, K. A. Biomolecular Coronas Provide the Biological Identity of Nanosized Materials. *Nat. Nanotechnol.* **2012**, *7*, 779-786.

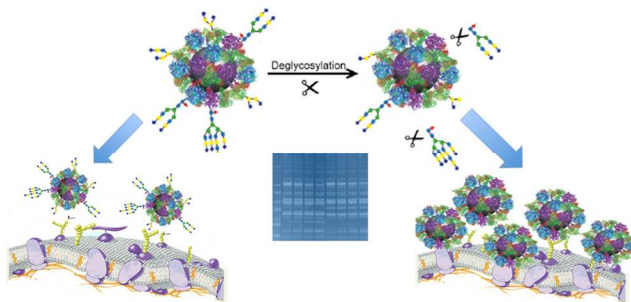
- 1
2
3
4
5
6
7
8
9
10
11
12
13
14
15
16
17
18
19
20
21
22
23
24
25
26
27
28
29
30
31
32
33
34
35
36
37
38
39
40
41
42
43
44
45
46
47
48
49
50
51
52
53
54
55
56
57
58
59
60
16. Treuel, L.; Brandholt, S.; Maffre, P.; Wiegele, S.; Shang, L.; Nienhaus, G. U. Impact of Protein Modification on the Protein Corona on Nanoparticles and Nanoparticle–Cell Interactions. *ACS nano* **2014**, *8*, 503-513.
17. Hu, W.; Peng, C.; Lv, M.; Li, X.; Zhang, Y.; Chen, N.; Fan, C.; Huang, Q. Protein Corona-Mediated Mitigation of Cytotoxicity of Graphene Oxide. *Acs Nano* **2011**, *5*, 3693-3700.
18. Han, X.; Corson, N.; Wade-Mercer, P.; Gelein, R.; Jiang, J.; Sahu, M.; Biswas, P.; Finkelstein, J. N.; Elder, A.; Oberdörster, G. Assessing the Relevance of in Vitro Studies in Nanotoxicology by Examining Correlations Between in Vitro and in Vivo Data. *Toxicology* **2012**, *297*, 1-9.
19. Maiorano, G.; Sabella, S.; Sorce, B.; Brunetti, V.; Malvindi, M. A.; Cingolani, R.; Pompa, P. P. Effects of Cell Culture Media on the Dynamic Formation of Protein–Nanoparticle Complexes and Influence on the Cellular Response. *ACS nano* **2010**, *4*, 7481-7491.
20. Aggarwal, P.; Hall, J. B.; McLeland, C. B.; Dobrovolskaia, M. A.; McNeil, S. E. Nanoparticle Interaction with Plasma Proteins as it Relates to Particle Biodistribution, Biocompatibility and Therapeutic Efficacy. *Adv. Drug Delivery Rev.* **2009**, *61*, 428-437.
21. Lesniak, A.; Fenaroli, F.; Monopoli, M. P.; Aberg, C.; Dawson, K. A.; Salvati, A. Effects of the Presence or Absence of a Protein Corona on Silica Nanoparticle Uptake and Impact on Cells. *ACS Nano* **2012**, *6*, 5845-5857.
22. Salvati, A.; Pitek, A. S.; Monopoli, M. P.; Prapainop, K.; Bombelli, F. B.; Hristov, D. R.; Kelly, P. M.; Aberg, C.; Mahon, E.; Dawson, K. A. Transferrin-Functionalized

- 1
2
3 Nanoparticles Lose Their Targeting Capabilities When A Biomolecule Corona Adsorbs
4 on the Surface. *Nat. Nanotechnol.* **2013**, *8*, 137-143.
5
6
7
8 23. Deng, Z. J.; Liang, M.; Monteiro, M.; Toth, I.; Minchin, R. F. Nanoparticle-Induced
9
10 Unfolding of Fibrinogen Promotes Mac-1 Receptor Activation and Inflammation. *Nat*
11
12 *Nanotechnol* **2011**, *6*, 39-44.
13
14
15 24. Fleischer, C. C.; Payne, C. K. Nanoparticle-Cell Interactions: Molecular Structure of the
16
17 Protein Corona and Cellular Outcomes. *Acc Chem Res* **2014**, *47*, 2651-2659.
18
19
20 25. Yan, Y.; Gause, K. T.; Kamphuis, M. M.; Ang, C. S.; O'Brien-Simpson, N. M.; Lenzo, J.
21
22 C.; Reynolds, E. C.; Nice, E. C.; Caruso, F. Differential Roles of the Protein Corona in
23
24 the Cellular Uptake of Nanoporous Polymer Particles by Monocyte and Macrophage Cell
25
26 Lines. *ACS Nano* **2013**, *7*, 10960-10970.
27
28
29 26. Bohne-Lang, A.; Von der Lieth, C. W. GlyProt: in Silico Glycosylation of Proteins.
30
31 *Nucleic Acids Res* **2005**, *33*, W214-W219.
32
33
34 27. Moremen, K. W.; Tiemeyer, M.; Nairn, A. V. Vertebrate Protein Glycosylation:
35
36 Diversity, Synthesis and Function. *Nat. Rev. Mol. Cell Biol.* **2012**, *13*, 448-462.
37
38
39 28. Paszek, M. J.; DuFort, C. C.; Rossier, O.; Bainer, R.; Mouw, J. K.; Godula, K.; Hudak, J.
40
41 E.; Lakins, J. N.; Wijekoon, A. C.; Cassereau, L.; *et al.* The Cancer Glycocalyx
42
43 Mechanically Primes Integrin-Mediated Growth and Survival. *Nature* **2014**, *511*, 319-
44
45 325.
46
47
48 29. Monopoli, M. P.; Walczyk, D.; Campbell, A.; Elia, G.; Lynch, I.; Baldelli Bombelli, F.;
49
50 Dawson, K. A. Physical-Chemical Aspects of Protein Corona: Relevance to in Vitro and
51
52 in Vivo Biological Impacts of Nanoparticles. *J. Am. Chem. Soc.* **2011**, *133*, 2525-2534.
53
54
55
56
57
58
59
60

- 1
2
3
4
5
6
7
8
9
10
11
12
13
14
15
16
17
18
19
20
21
22
23
24
25
26
27
28
29
30
31
32
33
34
35
36
37
38
39
40
41
42
43
44
45
46
47
48
49
50
51
52
53
54
55
56
57
58
59
60
30. Hühn, D.; Kantner, K.; Geidel, C.; Brandholt, S.; De Cock, I.; Soenen, S. J.; Rivera_Gil, P.; Montenegro, J.-M.; Braeckmans, K.; Müllen, K.; *et al.* Polymer-Coated Nanoparticles Interacting with Proteins and Cells: Focusing on the Sign of the Net Charge. *ACS Nano* **2013**, *7*, 3253-3263.
31. Walczyk, D.; Bombelli, F. B.; Monopoli, M. P.; Lynch, I.; Dawson, K. A. What the Cell "Sees" in Bionanoscience. *J. Am. Chem. Soc.* **2010**, *132*, 5761-5768.
32. Preston, R. J.; Rawley, O.; Gleeson, E. M.; O'Donnell, J. S. Elucidating the Role of Carbohydrate Determinants in Regulating Hemostasis: Insights and Opportunities. *Blood* **2013**, *121*, 3801-3810.
33. Swiss-Prot Database Entry # P02769.
34. Johnson, J. L.; Jones, M. B.; Ryan, S. O.; Cobb, B. A. The Regulatory Power of Glycans and Their Binding Partners in Immunity. *Trends Immunol.* **2013**, *34*, 290-298.
35. Nimmerjahn, F.; Ravetch, J. V. Anti-Inflammatory Actions of Intravenous Immunoglobulin. *Annu. Rev. Immunol.* **2008**, *26*, 513-533.
36. Tjiu, J.-W.; Chen, J.-S.; Shun, C.-T.; Lin, S.-J.; Liao, Y.-H.; Chu, C.-Y.; Tsai, T.-F.; Chiu, H.-C.; Dai, Y.-S.; Inoue, H.; *et al.* Tumor-Associated Macrophage-Induced Invasion and Angiogenesis of Human Basal Cell Carcinoma Cells by Cyclooxygenase-2 Induction. *J. Invest. Dermatol.* **2008**, *129*, 1016-1025.
37. Murray, P. J.; Allen, J. E.; Biswas, S. K.; Fisher, E. A.; Gilroy, D. W.; Goerdt, S.; Gordon, S.; Hamilton, J. A.; Ivashkiv, L. B.; Lawrence, T.; *et al.* Macrophage Activation and Polarization: Nomenclature and Experimental Guidelines. *Immunity* **2014**, *41*, 14-20.

- 1
2
3
4
5
6
7
8
9
10
11
12
13
14
15
16
17
18
19
20
21
22
23
24
25
26
27
28
29
30
31
32
33
34
35
36
37
38
39
40
41
42
43
44
45
46
47
48
49
50
51
52
53
54
55
56
57
58
59
60
38. Durafourt, B. A.; Moore, C. S.; Zammit, D. A.; Johnson, T. A.; Zaguia, F.; Guiot, M. C.; Bar-Or, A.; Antel, J. P. Comparison of Polarization Properties of Human Adult Microglia and Blood-Derived Macrophages. *Glia* **2012**, *60*, 717-727.
39. Chinetti-Gbaguidi, G.; Baron, M.; Bouhrel, M. A.; Vanhoutte, J.; Copin, C.; Sebti, Y.; Derudas, B.; Mayi, T.; Bories, G.; Tailleux, A.; *et al.* Human Atherosclerotic Plaque Alternative Macrophages Display Low Cholesterol Handling But High Phagocytosis Because of Distinct Activities of the PPAR γ and LXRA Pathways. *Circ. Res.* **2011**, *108*, 985-995.
40. Edin, S.; Wikberg, M. L.; Rutegård, J.; Oldenborg, P.-A.; Palmqvist, R. Phenotypic Skewing of Macrophages in Vitro by Secreted Factors from Colorectal Cancer Cells. *PloS One* **2013**, *8*, e74982.
41. Xia, T.; Kovochich, M.; Brant, J.; Hotze, M.; Sempf, J.; Oberley, T.; Sioutas, C.; Yeh, J. I.; Wiesner, M. R.; Nel, A. E. Comparison of the Abilities of Ambient and Manufactured Nanoparticles to Induce Cellular Toxicity According to An Oxidative Stress Paradigm. *Nano Lett.* **2006**, *6*, 1794-1807.
42. Shevchenko, A.; Wilm, M.; Vorm, O.; Mann, M. Mass Spectrometric Sequencing of Proteins Silver-Stained Polyacrylamide Gels. *Anal. Chem.* **1996**, *68*, 850-858.

TOC



1
2
3
4
5
6
7
8
9
10
11
12
13
14
15
16
17
18
19
20
21
22
23
24
25
26
27
28
29
30
31
32
33
34
35
36
37
38
39
40
41
42
43
44
45
46
47
48
49
50
51
52
53
54
55
56
57
58
59
60